Article:

Ozdemir Kilinc, Z., Hernandez-Nava, E., Tyas, A. et al. (5 more authors) (2016) Energy absorption in lattice structures in dynamics: Experiments. International Journal of Impact Engineering, 89. 49 - 61. ISSN 0734-743X

https://doi.org/10.1016/j.ijimpeng.2015.10.007

Energy absorption in lattice structures in dynamics: Experiments

Zuhal Ozdemir[a], Everth Hernandez-Nava[b], Andrew Tyas[a], James A. Warren[a], Stephen D. Fay[c], Russell Goodall[b], Iain Todd[b], Harm Askes[a,**]

[a]*Department of Civil and Structural Engineering, the University of Sheffield, UK*
[b]*Department of Material Sciences and Engineering, the University of Sheffield, UK*
[c]*Blastech Ltd, The Bio Incubator, 40 Leavygreave Street,Sheffield, UK*

Abstract

Lattice structures offer the potential to relatively easily engineer specific (meso-scale properties (cell level)), to produce desirable macro-scale material properties for a wide variety of engineering applications including wave filters, blast and impact protection systems, thermal insulation, structural aircraft and vehicle components, and body implants. The work presented here focuses on characterising the quasi-static and, in particular, the dynamic load-deformation behaviour of lattice samples. First, cubic, diamond and re-entrant cube lattice structures were tested under quasi-static conditions to investigate failure process and stress-strain response of such materials. Following the quasi-static tests, Hopkinson pressure bar (HPB) tests were carried out to evaluate the impact response of these materials under high deformation rates. The HPB tests show that the lattice structures are able to spread impact loading in time and to reduce the peak impact stress. A significant rate dependency of load-deformation characteristics was identified. This is believed to be the first published results of experimental load-deformation studies of additively manufactured lattice structures. The

*Corresponding author
**Tel. +44(0)114 222 5769; Fax: +44(0)114 222 5700
Email address: h.askes@sheffield.ac.uk (Harm Askes)

cubic and diamond lattices are, by a small margin, the most effective of those lattices investigated to achieve this.

Keywords: lattice structures, impact and blast protection, Hopkinson pressure bar (HPB)

1. Introduction

The choice of material for a given structural problem requires a careful balance of strength, stiffness, cost, durability and relative static and dynamic properties. Lattice structures are multi-functional materials that can offer a range of these desirable properties. They are commonly constructed by duplicating three-dimensional meso-scale unit cells, typically at the scale of a few mm. The stiffness and strength of these materials depend on relative density, strut aspect ratio (radius/length), unit cell geometric configuration, unit-cell size, properties of parent material, and rate of loading (Ashby, 2006). By changing the spatial configuration of struts and/or strut diameters, different geometries with different material properties can be produced, which will be explored herein the context of protection against blast and impact loading.

Although lattice structures are different from cellular materials, certain concepts carry over from the well-studied cellular materials to the less well-know lattice structures, especially under transient dynamic loading conditions. It is thus worthwhile to review briefly the state of the art in cellular materials.

Properties of cellular materials have been the subject of many studies (Reid et al. (1983), Stronge and Shim (1987), Reid and Peng (1997), Deshpande and Fleck (2000), Elnasri et al. (2007)). The mechanical response of cellular materials under intense blast and impact loading may result in localisation of deformation, densification and material resistance and stiffness leading to propagation of the deformation by a process akin the development of shock waves; this extreme localisation is typical for "sparse materials" (Harrigan et al. (2010)) and not observed in bulk materials. In cellular solids, shock wave propagation is frequently studied using one-dimensional analytical models, spring-mass models or finite element (FE) models. Reid et al. (1983) developed a theory for the propagation of structural shock waves through one-dimensional metal ring systems in order to explain the experimentally observed behaviour of such structures when subjected to end impact. More detailed dynamic crushing experiments on tightly packed arrays of thin-walled metal tubes were carried out by Stronge and Shim (1987). Reid and Peng (1997) evaluated the enhancement of crushing strength of wood samples under high velocity impact with a rate-independent simple shock wave model. Since the cell sizes within wood are very small, the material behaviour was homogenized by assuming a rigid perfectly plastic locking (RPPL) material model for wood to determine the strength enhancement due to shock wave propagation. Two important parameters, namely plateau stress σ_{pl} and densification or lock-up strain ϵ_{D}, were used to characterize the constitutive behaviour of the material. By assuming a certain level of strength enhancement, critical impact velocities, at which shock propagation effects become important and the response becomes dependent upon the impact velocity, were defined (e.g. Deshpande and Fleck (2000) adopted a criterion of a 20 % elevation in strength for foams). Since these parameters cannot be easily identified from stress-strain data for shock enhancement prediction, a simple power law densification model was proposed to replace the RPPL model (Pattofatto et al., 2007). Tan et al. (2005) used the efficiency of cellular material in absorbing energy to compute σ_{pl} and ϵ_{D}.

In addition to shock wave propagation, strength increase in cellular solids under dynamic loading conditions may be attributed to micro-inertial effects (Deshpande and Fleck, 2000). Bending dominated (Type I) structures with flat topped quasi-static stress-strain curve are slightly affected by micro-inertial effects under dynamic conditions. Metallic foams generally behave as Type I structures. Deshpande and Fleck (2000) verified rate insensitive behaviour of two particular types of aluminium foam under high strain rates by split Hopkinson pressure bar (HPB) and direct impact tests. Elnasri et al. (2007) reported the existence of shock front in cellular structures under high strain rate impact loading at low critical velocities by comparing the results of direct Hopkinson bar and Hopkinson bar-Taylor tests. On the other hand, stretch dominated (Type II) structures show sharp softening behaviour after peak load. In contrast to bending dominated structures, stretch dominated structures are significantly influenced by micro-inertial effects (Calladine and English, 1984). Strength enhancement of square tubes in successive folding mechanisms under impact loading was attributed to the higher strain in edge-areas of the tube because of inertia (Zhao and Abdennadher, 2004).

Recent technological advances, i.e. additive manufacturing techniques, allows us to create periodic metallic lattice structures with an efficient geometry which, in principle, can minimise the material usage whilst optimising the desired mechanical properties of the material. One potentially promising application is the use of bespoke metallic lattices as sacrifically energy-absorbing layers in protection systems against blast and impact loading. However, as a sub-class of cellular solids, lattice structures are quite new materials for blast, ballistic and impact protection applications, and experimental and numerical studies on the dynamic response of such materials are very limited. McKown et al. (2008) experimentally evaluated the quasi-static response and dynamic progressive collapse behaviour of steel lattice structures under impulsive loads and their associated failure modes, without focusing on the effect of lattice structures on the temporal spreading of impulse. Hasan et al. (2010) compared the drop weight impact performance of sandwich panels with aluminium honeycomb and titanium alloy lattice structures in terms of specific impact energy versus dent depth. Smith et al. (2010) conducted an extensive study to characterise the response of steel lattice structure samples to blast. They presented quantitative deformations of qualitative damage as a function of blast impulse. However, to date, no experimental data on the dynamic load-displacement characteristics of cellular metallic lattice materials has been presented in the literature.

In the current work, the energy absorption behaviour and failure modes of lattice structures under quasi-static and dynamic loading conditions are studied. In order to maximise the freedom in creation of potentially complex lattice structures, additive layer manufacturing techniques, where a structure is built up progressively by the selective melting of specific regions in successive layers of metal powder are used. Titanium alloy (Ti6Al4V) is preferred, due to its high specific properties, and availability of data to allow modelling of mechanical response (U.S. Department of Transportation Federal Aviation Administration DOT/FAA/AR-00/25, 2000), (Shao et al., 2010). Lattice structures with different unit cell geometries are fabricated using the Electron Beam Melting (EBM) technique. A series of experimental tests performed on the lattice structure samples. First, the load-deflection response and associated failure modes of such structures were captured by quasi-static compression tests. Following the compression tests, the impact response of lattice structures under high deformation rates was evaluated by HPB tests to assess the ability of such materials to spread impact loading in time and to attenuate peak response.

The outline of this paper is as follows. Section 2 summarizes the manufacturing process of lattice structures. In Section 3, quasi-static stress-strain curves and associated failure modes of lattice structure samples are assessed. The experimental impact response of lattice structure samples is discussed in Section 4. Finally, in Section 5 some implications of the work are discussed.

A numerical modelling study of the quasi-static and dynamic collapose of these lattice materials has been conducted in parallel and the results of this will be published in a forthcoming paper.

2. Manufacturing process

A range of Additive Manufacturing techniques have been developed, and equipment is commercially available. The names used vary with equipment supplier, and there are fundamental differences between some of the techniques; for example, Selective Laser Melting (SLM) uses a laser as the directable heat source, while Electron Beam Melting (EBM) uses a high-energy beam of electrons. In this case EBM has been selected for use as the beam can be split and moved around the build area more rapidly, meaning samples can be produced in less time. The EBM technique can be used for the production of metallic materials of arbitrary shape. This technique does not require additional treatments (thermal, machining etc) to obtain the final shape or mechanical properties (Al-Bermani et al., 2010).

In this work, lattice samples are manufactured from spherical grade 5 Ti6Al4V powder with 45-110 µm particle size using an ARCAM S12 EBM machine. Three unit cell geometries of increasing complexity, shown in Figure 1, are chosen for the lattice samples. For the cubic lattice geometry (Figure 1-(a)), struts run along the edges of the unit cell. The other geometries are diamond (Figure 1-(b)), where the struts are arranged in directions similar to the interatomic bonds in the atomic lattice of diamond, and re-entrant cube (Figure 1-(c)), where all edges and diagonal struts across the faces bent towards the centre. The repeating unit cell is kept as a 5 mm side length cube for all three lattice structures. Square strut cross-sections were chosen for the cubic and diamond lattices with diagonal lengths of 1.3 and 1.0 mm, respectively, whereas the strut diameter of the re-entrant cube is 0.48 mm. Figure 2 shows single layer cubic, diamond and re-entrant cube samples prior to testing.

Figure 3 presents Scanning Electron Microscopy (SEM) images of an individual unit-cell strut of a diamond lattice specimen. The layered nature of a strut along the length and its roughly square cross-section can be observed in Figures 3-(a) and (b).

The relative density $\bar{\rho}$, which is the ratio of the measured lattice density ρ to the density of the titanium alloy ρ_s, is given by:

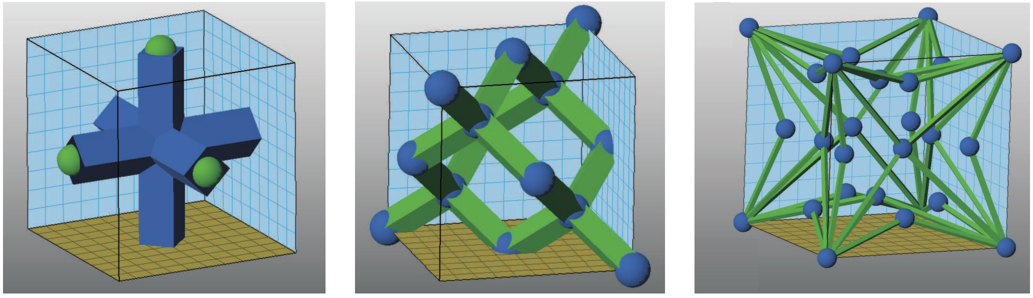

(a) (b) (c)

Figure 1: Representative unit cells of (a) cubic, (b) diamond and (c) re-entrant cube lattice structures. When built, the unit cell side length in the lattices is 5 mm.

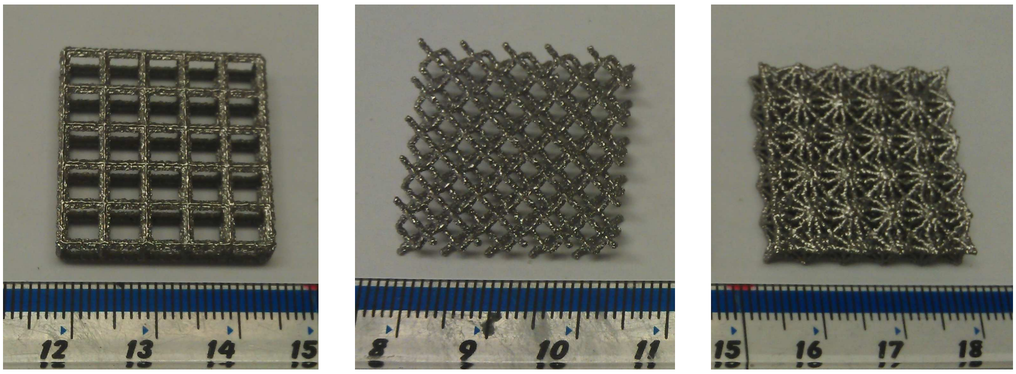

(a) (b) (c)

Figure 2: View of single layer (a) cubic, (b) diamond and (c) re-entrant cube lattice structures prior to testing

$$\bar{\rho} = \frac{\rho}{\rho_s} \tag{1}$$

Relative densities of the ideal structures for cubic, diamond and re-entrant

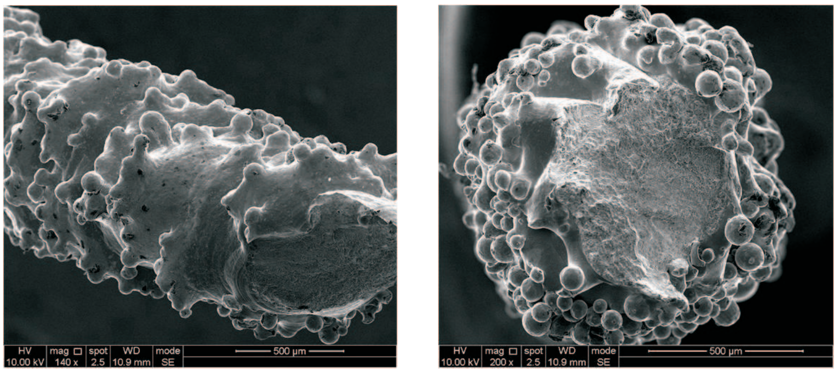

(a) (b)

Figure 3: SEM photographs of (a) an individual unit-cell strut along the strut length, (b) its square cross-section

cube unit cells are 0.139, 0.137 and 0.166, respectively.

3. Quasi-static response of lattice structures

Single-layer and five-layer samples of lattice structures were tested under conventional quasi-static conditions using a Houndsfield TX0038 universal test rig with compression platens which were verified before testing to have a misalignment below 0.5°.

3.1. Quasi-static response of single layer lattice structures

Single layer square samples of lattice structures with edge length of 25 mm and a height of 5 mm were compressed at a crosshead speed of 0.2 mm/min. For each sample type, three quasi-static tests were carried out. The engineering stress-strain curves of cubic, diamond and re-entrant cube lattice structure samples following the quasi-static compression tests are shown in Figure 4. Initial offset, due to some of the struts coming into contact with the test platens before others, as either the samples are not exactly rectilinear, or they are not exactly aligned, is eliminated from the experimental stress-strain curves.

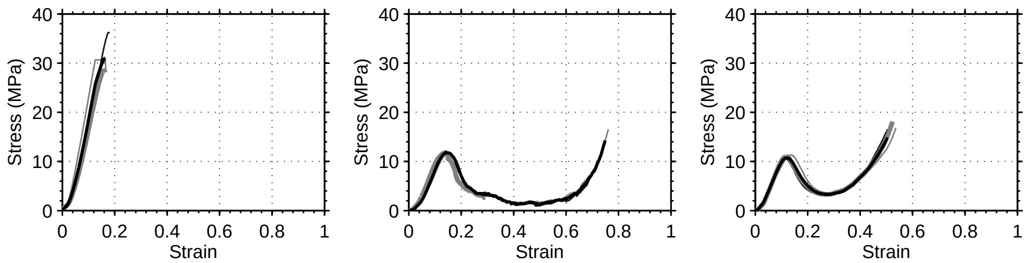

(a) (b) (c)

Figure 4: The engineering stress-strain curves of single-layer (a) cubic, (b) diamond and (c) re-entrant cube samples obtained following compression test 1 (thin grey line), test 2 (thin black line) and test 3 (thick grey line), and average of these curve (thick black line).

The quasi-static stress-strain response of the cubic lattice structure, shown in Figure 4a, is effectively elastic before brittle failure; this is to be expected, from the unit cell geometry, which does not encourage plastic deformation. Instead, the failure mechanism is similar to that shown for a brittle foam by Ashby (2006), with shear fracture occurring at the joints between the longitudinal and lateral struts. The diamond Figure 4b and re-entrant Figure 4c unit cell stress-strain relationships show a relatively constant initial stiffness, followed by post-peak softening, and later stiffness increase due to final densification of the material. This is typical of Type II (stretch dominated) response which appears to be the predominant deformation characteristic of the diamond lattice. However, in the case of the re-entrant lattice structure unit cell, pronounced post-peak softening is observed despite the deformation involving significant flexural deformation, because the re-entrant geometry leads to a loss in stiffness once rotation of the nodes commences.

3.2. Quasi-static response of multi-layer lattice structures

Next, five-layer square samples (each consisting of 5 by 5 unit cells) of diamond and re-entrant cube lattice structures with an edge length of 25 mm and a height of 25 mm were manufactured to be tested at a cross-head speed of 0.2 mm/min and 0.1 mm/min, respectively. The stress-strain curves of lattice structure samples following quasi-static compression tests are shown in Figure 5. The curves show distinct peaks at low platen displacements for both diamond and re-entrant cube samples. At higher platen displacements, peaks become less clear. Each of these peaks observed on the stress-strain curve of the re-entrant cube lattice structures corresponds to the failure of one particular layer at a time; however, this failure of layers occurs in an arbitrary order. Small deviations are observed between stress-strain curves carried out on different samples. Peak responses of single and multi-layer re-entrant cube samples are very close. Therefore, re-entrant lattice structures exhibit more predictable behaviour. Compared to re-entrant cube samples, the deformation of diamond lattice structures is less constrained by the particular configuration of struts, and therefore their stress-strain curves show a more random behaviour. Failure in diamond lattice structures develops and propagates in the weakest parts of the sample. Load is resisted by a longer diagonal path in five-layer diamond lattices, see also Figure 6 below. Therefore, the peak response of the five-layer diamond lattices is higher than that of single-layer samples.

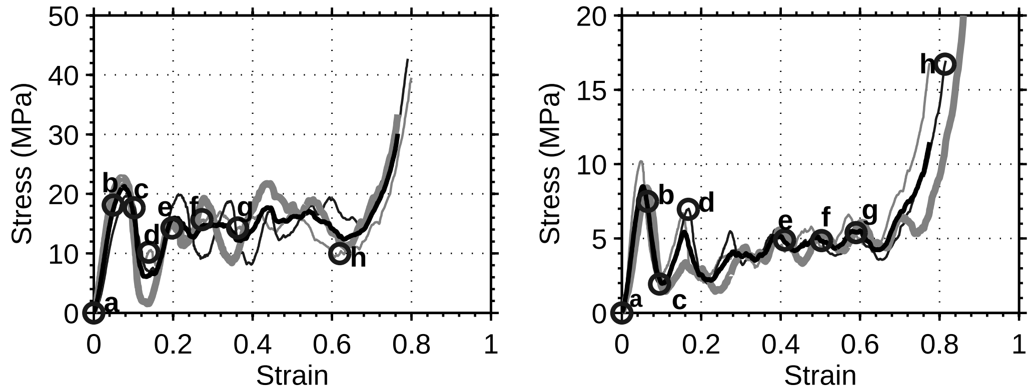

(a) (b)

Figure 5: The stress-strain curves of five-layer (a) diamond and (b) re-entrant cube samples obtained following the compression test 1 (thin grey line), test 2 (thin black line) and test 3 (thick grey line), and average of these curves (thick black line).

The stress-strain responses of the diamond lattice structures shown in Figure 5-(a) is correlated with the images taken during the compression test in Figure 6. Each of these images corresponds to a different point on the force-displacement curve of compression test 1. Figure 6-(a) shows the undeformed diamond sample. The onset of the failure of the struts at the first layer is shown in Figure 6-(b). Figure 6-(c) illustrates failure of struts touching the bottom platen. Figure 6-(d) corresponds to the onset of the development of localised failure of struts along a diagonal on the lower right part of the sample. As the sample is more compressed, shear failure becomes clearer (Figures 6-(e) and (g)). Figure 6-(h) corresponds to the onset of densification.

The images taken during the compression test of a re-entrant cube sample are shown in Figure 7. Again, each of the images corresponds to a different point on the force-displacement curve of compression test 2 shown in Figure 5-(b). The undeformed sample is shown in Figure 7-(a). Figure 7-(b) illustrates the onset of failure of the struts at the first layer. Load on the second layer starts increasing after point (c) as shown in Figure 5-(b). The onset of the failure of the struts at the second layer of the re-entrant cube sample coincides with point (d) as represented on Figure 7-(d). Figures 7-(e) and (f) show failure of the third layer. The onset of failure of the final layer of the sample is given in Figure 7-(g). Figure 7-(h) shows the state of the sample during densification. Comparing Figures 6 and 7, it is clear that failure of the re-entrant lattice occurs in a much more systematic, layer-by-layer fashion than failure of the diamond lattice.

Elastic modulus E, yield stress σ_{y} and absorbed energy (up to densification) of the single and multi-layer samples obtained following the quasi-static tests are summarized in Table 1. This table also gives the actual density of the lattices, which matches the density of the designed structures very well. It must nevertheless be noted that processing defects can lead to departures in some additively manufactured porous materials (Hernandez-Nava et al., 2015), and that test orientation relative to build direction (which was constant here) can also have an effect (Amendola et al., 2015). Strain limits up to 30 % and 60 % are chosen to compute absorbed energy for the single-layer re-entrant cube lattices and other sample types, respectively. These values

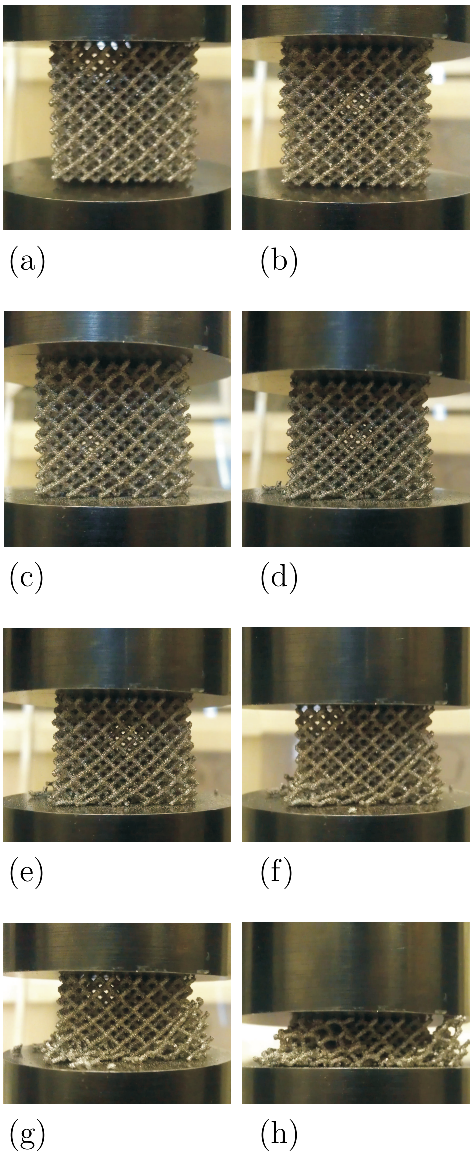

Figure 6: The images taken during the quasi-static compression test of the five-layer diamond sample correspond to the points of stress-strain curve observed during compression test 1 as shown in figure 5-(a).

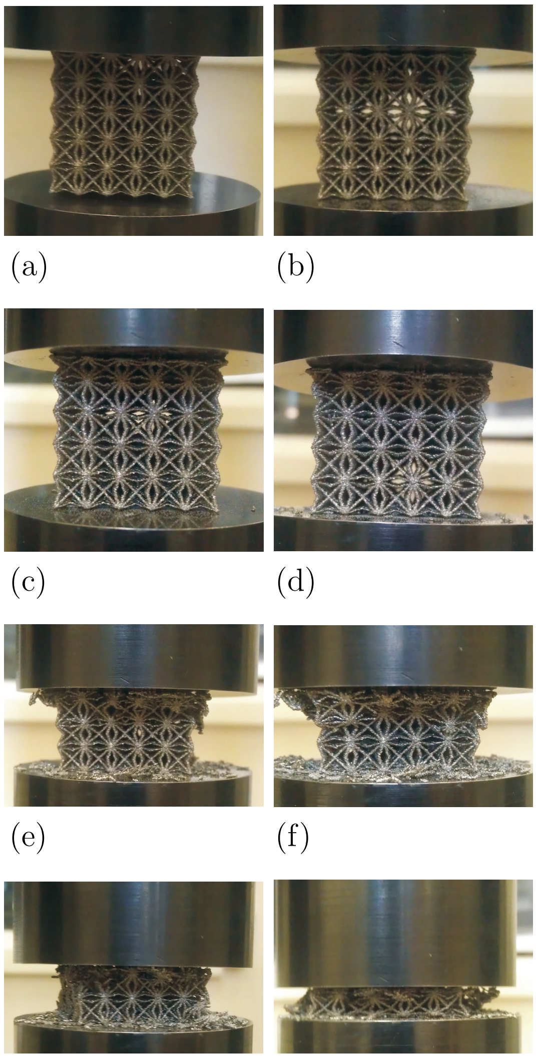

(a) (b) (c) (d) (e) (f) (g) (h)

Figure 7: The images taken during the quasi-static compression test of the five-layer re-entrant cube sample correspond to the points of stress-strain curve observed during compression test 2 as shown in figure 5-(b).

are chosen such that the unbounded energy absorption associated with the densification stage is ignored. The multi-layer samples offer a significantly higher elastic modulus than the single-layer samples. A tentative explanation for this unexpected phenomenon could be the difference in stiffness between internal layers and boundary layers. Internal layers can be expected to have full stiffness, whereas boundary layers are weakened by imperfect contact conditions and buckling of struts in the contact zone, especially for the diamond samples. In multi-layer samples, the stiffness reducing effects of the boundary layers are relatively less important, thus the overall stiffness is larger than for a single-layer sample. Similarly, the yield stress of diamond lattices increases significantly with the number of layers, while re-entrant cube lattices do not exhibit such behaviour. Diamond samples can absorb more energy than re-entrant cube samples under quasi-static conditions, although the relative density of the re-entrant cube samples is higher than that of diamond lattices. Both explanations require further study, possibly by studying samples with different number of layers.

4. Impact characteristics of lattice structures

The impact response of lattice structures under high deformation rates was evaluated by HPB tests. The motivation behind all the tests is to investigate how the presence of a lattice structure specimen influences the load-time history generated by the impact of the projectiles described below. Tests were first carried out in the absence of the lattice specimen at the impact face of the HPB to establish baselines for the loading generated by the bare impactor. Impact tests were then repeated in the presence of

Lattice structure	N. of layers	$\bar{\rho}$	E	σ_{y}	Absorbed energy
		[$-$]	[MPa]	[MPa]	[MJ/m^3]
Diamond	1	0.137	132.2	11.8	2.32
Diamond	5	0.137	399.5	21.3	8.39
Re-entrant cube	1	0.166	126.6	10.8	1.65
Re-entrant cube	5	0.166	216.4	8.51	2.51

Table 1: Averaged material properties obtained following the quasi-static tests.

single layer lattice structures of the same diameter as the impactor in order to establish the ability of the lattice structures to extend the duration of the impact load and to reduce peak response. Finally, five-layer samples are used to examine the temporal spreading of load.

4.1. Rationale for choice of impact loading

Suitable magnitudes and rates of loading for the impact tests were identified considering a 10 kg TNT detonation at distances of 1.75 m and 2.5 m. This would produce specific reflected impulses of 9000 and 3000 kPa · msec, respectively (Hyde (1991)). If these impulses were imparted to a steel plate target of thickness 5 mm, the resulting kinetic energies areal density in the plate would be in the range 100-1100 kJ/m^2. The same order of magnitude kinetic energy and impulse can be imparted to the target lattice specimens using a steel bar projectile or a Nylon 66 impactor in order to differentiate between low and high velocity impact. In this study, we have used a 25 mm diameter and 250 mm long EN24T steel bar with mass of 963 g fired at velocities in the range 5-21 m/s for *low-velocity* impact tests, as well as a 27 mm diameter and 31 mm long Nylon 66 projectiles with mass of 19.3 g fired at velocities in the range 80-250 m/s for *high-velocity* impact tests. The specific impulse and kinetic energy density delivered to the target specimen was thus in the range 10000-40000 kPa $\cdot$ msec and 25-400 kJ/m^2 for the steel bar impactor and 3000-9000 kPa $\cdot$ msec and 115-1150 kJ/m^2 for the Nylon 66 impactor. All impacts were conducted by firing projectiles from a single stage gas gun.

4.2. The HPB Test set-up

Impact response of lattice structures under high deformation rates was evaluated using HPB tests. The Hopkinson pressure bars used in this work were all custom made, from EN24(T) cylindrical bar. All bars are 3.4 m long and have a 0.025 m diameter. Optical records of all tests were recorded by a Phantom v 4.2 high speed digital video camera with 256 x 112 pixels, operating typically at 40-50 μs per frame. The velocity of the impactor during the impact event and the displacement vs time record of the compressed specimens can therefore be established using the high speed video footage.

A single strain gauge station positioned 250 mm from the impact face of each bar, comprising 4 orthogonally placed high gauge factor Kyowa KSP-2-120-E4 semi-conductor strain gauges, linked in such a way as to eliminate bending effects in the output strain. The output of the strain gauge stations checked by the application of a known impulse which was compared to the integrated load-time data at the strain gauge station, by means of an impact test with a known impact mass and impact/rebound velocities of the impactor recorded using a high speed digital video camera. Density and elastic modulus of the bars were determined using elastic wave propagation tests, and found to be 7850 kg/m^3 and 210.2 GPa, respectively.

It is possible in principle to perform frequency domain correction of the signals recorded at a strain gauge station on the bar to account for dispersion effects as the pulse propagates along the bar, and hence to reconstruct the load-time history at the impact face of the bar. However, it is known that there is an upper limit to the frequency of Fourier components for which standard dispersion correction methods are applicable. Tyas and Watson (2001) note that this upper limit is $1250/a$ kHz, where a is the radius of the bar in mm. In the experimental signals recorded in this study, there was typically significant energy present at frequencies well in excess of this value, and therefore dispersion correction was not applied. Instead, the dispersed signals recorded at the strain gauge location in the experimental work are presented.

Two testing configurations were considered for the HPB tests: In the first case, the specimen was placed on the impact face of the HPB and the projectile was fired onto the specimen. Therefore, the strain gauge station recorded the strain on the distal face of the lattice structure specimen (Figure 8-(a)). This test configuration is called a distal-face test. In the other case, the test specimens were fixed to the impact face of the projectile (Figure 8-(b)). In these tests, the stress recorded on the face of the HPB was from the impact face of the specimen which experiences a sudden change of velocity on impact. This test configuration is called an impact-face test. The purpose of these tests and their comparison is to determine whether the stress in the specimen was effectively uniform throughout the specimen length, or whether there were significant variations between the distal and impact faces. The difference between the impact and distal face loads shows the effectiveness of the lattice structures were they to be used as a cushioning layer to protect rear structure. The specimens were laterally unconfined in all cases. No correction was made for dispersion in propagation of the pulse from the impact face of the HPB to the strain gauge station.

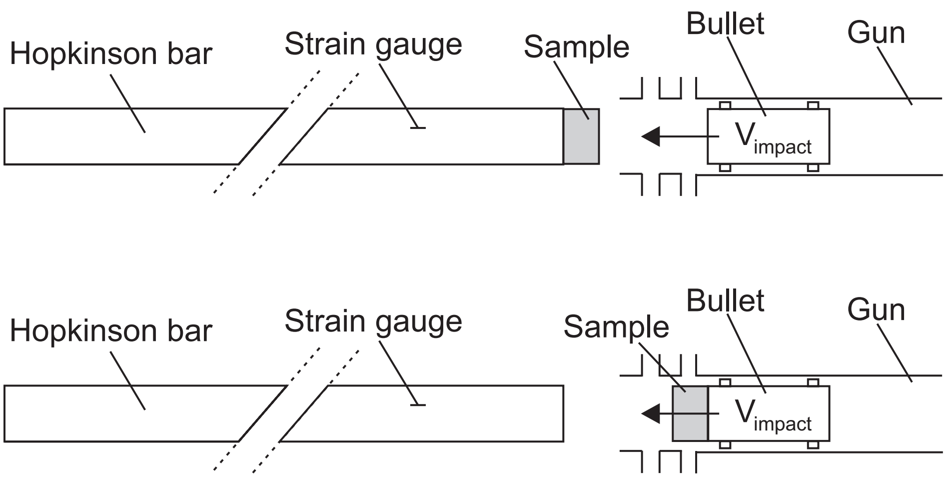

(a)

(b)

Figure 8: Two testing configurations for the HPB tests: (a) the distal face test and (b) impact face test.

4.3. The HPB tests in the absence of lattice structure specimens

These tests were conducted to establish the baseline impact stress-time histories when the impactors struck the HBP with no lattice structure specimen present. Tests were carried out using the steel impactor at velocities of 7.3-8.9 m/s and the Nylon 66 projectiles at velocities of 175-191 m/s. Examples of typical stress-time histories are shown in Figure 9.

The key points to note here are the high magnitude of the peak stresses, which are 135 MPa for the steel impactor and 240 MPa for the Nylon 66 impactor, and the very short durations of the main impact pulse of 50-100 μs. For the case of the steel impactor, the main impact is followed by a small amplitude stress pulse. This verifies that the impactor hits the HPB obliquely with a very small angle due to experimental errors in alignment. For the case of the Nylon 66 projectile, two peaks in the impact stress time history (Figure 9-(b)) show that the impactor undergoes inelastic deformations. It should be noted that these two peaks were cropped during the measurement.

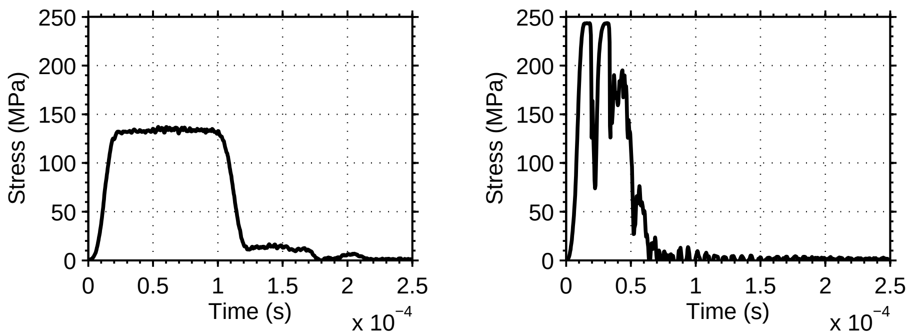

(a) (b)

Figure 9: Impact stress time histories in the absence of lattice structure specimen generated by the (a) steel and (b) Nylon 66 impactors fired at velocities of 7.6 and 178 m/s, respectively.

4.4. The HPB tests on single layer specimens

This group of tests were conducted on 5 mm thick cylindrical single layer re-entrant cube samples, with diameter 25 mm. Examples of stress and cumulative impulse time histories developed on the distal and impact faces induced by the steel impactor and the Nylon 66 projectile are shown in Figures 10 and 11, respectively. Cumulative impulse time histories are obtained by calculating the area under the impact force versus time plot. Impulse starts to increase when the impactor comes into contact with the HPB and remains unchanged following the rebound of the impactor.

Taking into account the difference in impact velocity from test to test, the impact and distal face stress-time histories from both the low-velocity and high-velocity impact tests are quite similar (Figures 10 and 11).

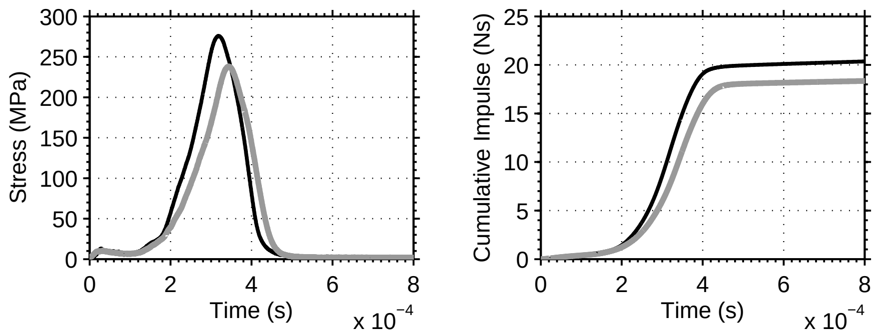

(a) (b)

Figure 10: Distal face (black line) and impact face (grey line) (a) stress and (b) cumulative impulse time histories of the single layer re-entrant cube lattice structure specimen induced by the steel impactor fired at velocities of 18.8 and 17.7 m/s, respectively.

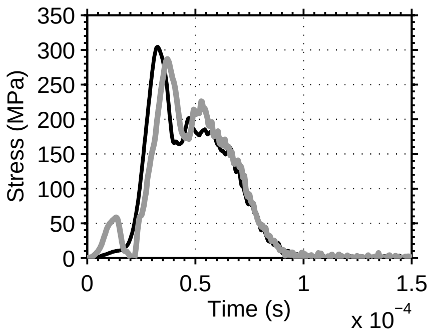

(a)

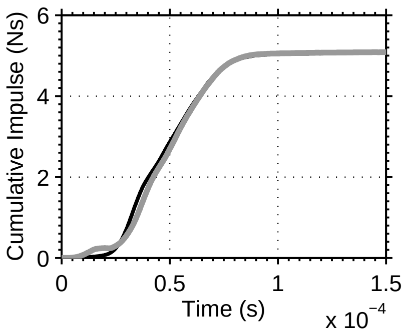

(b)

Figure 11: Distal face (black line) and impact face (grey line) (a) stress and (b) cumulative impulse time histories of the single layer re-entrant cube lattice structure specimen induced by the Nylon 66 impactor fired at velocities of 200 and 187 m/s, respectively.

4.5. The HPB tests on five-layer specimens

Cylindrical samples of nominal dimensions 25 mm long by 25 mm diameter were used to test the ability of the lattice structures to laterally spread impact load. First, distal face impact stress-time histories of five-layer cubic, diamond and re-entrant cube samples are compared in order to find out the most effective lattice type for impact protection. Examples of typical stress and cumulative impulse time histories for lower and higher end velocities of the two impactors are shown in Figures 12-15. In all cases, the presence of the lattice specimen significantly attenuates the peak impact stress transmitted to the bar, and significantly extends the duration of the load pulse. In the case of the low velocity steel impactor tests (7-9 m/s), the peak stress is reduced to around 20 % of that experienced in the bare impact tests whilst the duration of the load pulse is increased by around 2000 %.

In the higher velocity Nylon 66 projectile tests (170-190 m/s), the peak stress is attenuated to $\sim$ 35 % compared to the bare impact test by cubic and diamond micro-lattice samples, and to $\sim$50% by the re-entrant cube specimen. The duration of the load was extended by $\sim$350 % by the cubic and diamond specimens and by $\sim$250 % by the re-entrant cube specimens. The cubic and diamond lattices appear to be marginally more efficient in temporally spreading the load than the re-entrant cube lattice. This difference would be magnified on a weight-specific basis, as the re-entrant cube specimens have higher density.

In the low kinetic energy tests (i.e. the low velocity 7-9 m/s- steel impactor tests), the specimens experienced plastic work or damage along only part of their lengths and consequently the specimen did not begin to densify and stiffen, a process well known from quasi-static testing of foams and lattices generally, which occurs as the lattice structure collapses and the specimen density begins to approach that of the parent metal (Figure 12). In more energetic impacts (the high velocity 16-20 m/s- steel impactor tests) the cellular structure collapsed along the entire length of the specimen and densification begins to occur as the specimen loses its energy dissipation capacity (Figure 13). Thus, the specimen stress-time curve comprises a reasonably constant plateau load during cell collapse, followed by a much greater magnitude stress spike towards the end of the pulse. This feature is even more pronounced in the very high energy impacts of the Nylon 66 projectiles (Figures 14 and 15). In all cases, oscillations can be seen on the plateau load. The high speed video records shows that these oscillations are associated with the collapse of the individual cell layers. Similar features were seen on the traces from all the specimen types.

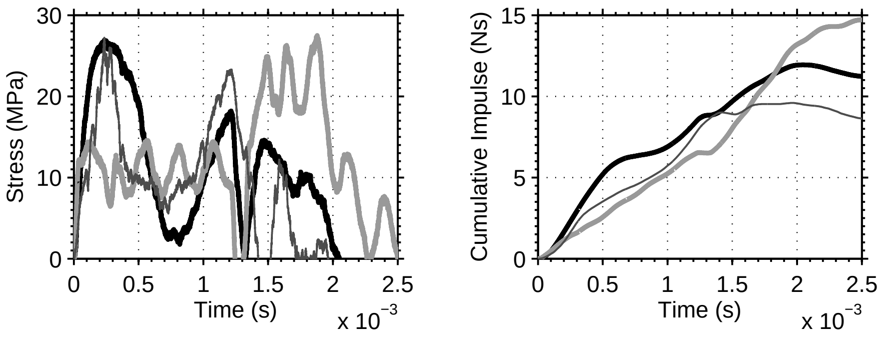

(a) (b)

Figure 12: Experimental distal face (a) stress and (b) cumulative impulse time histories of the five-layer cubic (thin black), diamond (thick black) and re-entrant cube (thick grey) lattice structure specimens induced by the steel impactor fired at velocities of 7.4 , 7.7 and 9.4 m/s.

Examples of the impact face stress compared to the distal face stress measurements developed on the diamond and re-entrant cube samples are shown in Figures 16–19. Considering the difference in impact velocity from test to test, the impact and distal face stress-time histories from the low-velocity steel impactor tests are quite similar (Figures 16 and 18). For both lattice types, the plateau stress is approximately equal at the two faces, indicating that this is purely a function of the resistance of the lattice. There are differences in the densification spike, but these may be explained primarily through differences in the impact velocity.

At higher velocity, there is a marked difference between the distal and impact face loads, unlike in single-layer samples (Figures 17 and 19). In

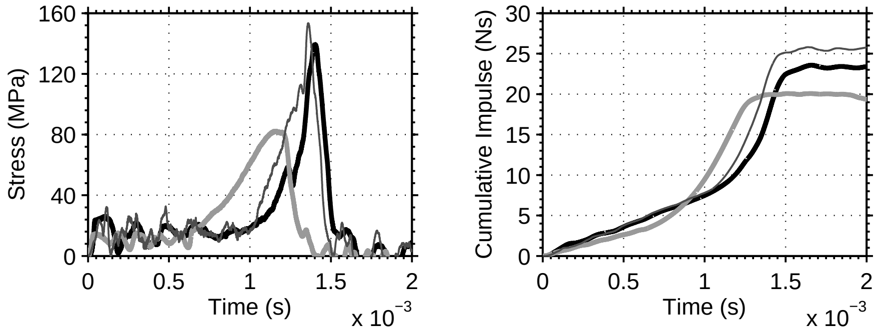

(a) (b)

Figure 13: Experimental distal face (a) stress and (b) cumulative impulse time histories of the five-layer cubic (thin black), diamond (thick black) and re-entrant cube (thick grey) lattice structure specimens induced by the steel impactor fired at velocities of 20.6, 19.4 and 16.8 m/s.

the case of the diamond lattice, the impact face load shows a pronounced initial peak, followed by a plateau load which is some 60-75% greater than the plateau load measured on the distal face in a slightly slower impact. The final densification peak is also significantly higher in magnitude than that measured at the distal face. In the case of the re-entrant cube lattice, the difference is even more pronounced. The impact face load shows a series of five clear peaks prior to the final densification peak. These peaks are assumed to be associated with the collapse of the five individual cell layers. The distal face trace shows a smooth plateau load followed abruptly by the densification peak. Similar behaviour was observed on the single layer samples.

Analysis of the high speed video footage shows that, in the lower velocity (steel impactor) tests, the failure of cell layers does not occur sequentially

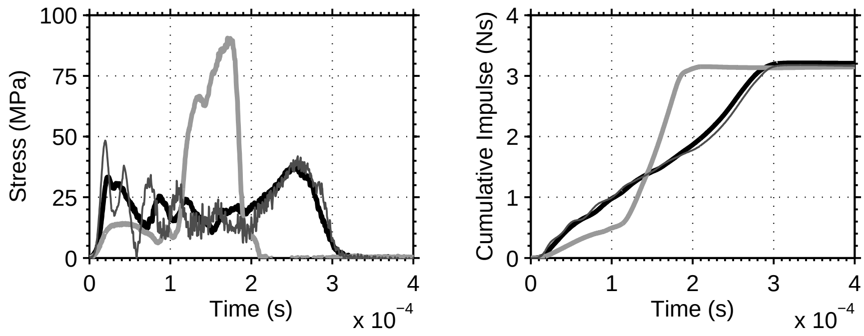

(a) (b)

Figure 14: Experimental distal face (a) stress and (b) cumulative impulse time histories of the five-layer cubic (thin black), diamond (thick black) and re-entrant cube (thick grey)lattice structure specimens induced by the Nylon 66 impactor fired at velocities of 130, 140 and 134 m/s.

from one end to the other. Instead, the order of cell layer collapse appears random similar to the quasi-static tests of Section 3. Figure 20 shows a example of this non-sequential collapse in the re-entrant cube specimen taken during the distal face HPB test where the steel impactor was fired at velocity of 16.8 m/s. Red arrows on the images show the compressing layer. As can be seen from these images, numbering the layers from left to right, the sequence of collapse of layers is one, four, three, two and five. It is likely that when the loading is applied sufficiently slowly for the entire length of the specimen to experience roughly equal load, the order of cell layer collapse is governed by the relative strength of the cell layers and small strength perturbations (caused, for example by variations in strut thickness along the length, as can be seen in Figure 3) lead to a random order of collapse. This is evidenced by

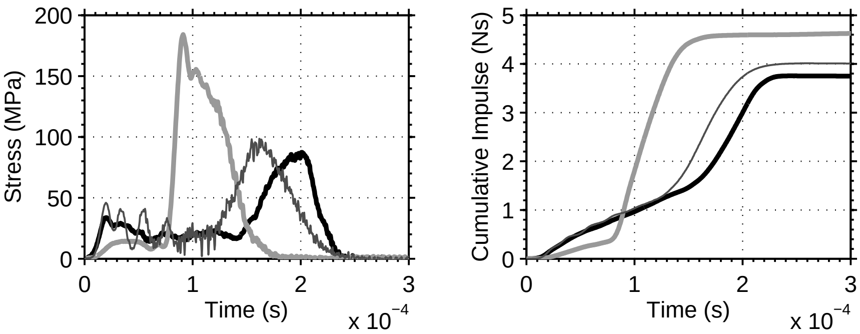

(a) (b)

Figure 15: Experimental distal face (a) stress and (b) cumulative impulse time histories of the five-layer cubic (thin black), diamond (thick black) and re-entrant cube (thick grey) lattice structure specimens induced by the Nylon 66 impactor fired at velocities of 195, 178 and 190 m/s.

the near equivalence of the distal and impact face loads. Similar behaviour is observed generally in the quasi-static testing of foams Tan et al. (2005).

Conversely, high speed video footage of the higher velocity (Nylon 66 impactor) tests shows the cell layer collapse invariably running from impact face to distal face. Figure 21 shows a example of this layer-by-layer collapse in the re-entrant cube specimen taken during the distal face HPB test where the Nylon 66 impactor was fired at velocity of 104.0 m/s. This indicates that equilibrium of load throughout the length of the specimen is not established at these higher velocities. The initial elastic deformation propagates through the specimen at high speed, resulting in the distal face approaching its plateau load. However, collapse is initially localized at the impact face, until such time as the cell layer at the impact face has densified and stiffened, produced increased resistance to the impact and propagated the deformation to the next cell layer. Hence, whilst the impact face sees a series of high load spikes due to the collapse and partial densification of each cell layer, the distal face sees only the initial, pre-collapse elastic load until the collapse is driven through to the final cell layer at the distal face.

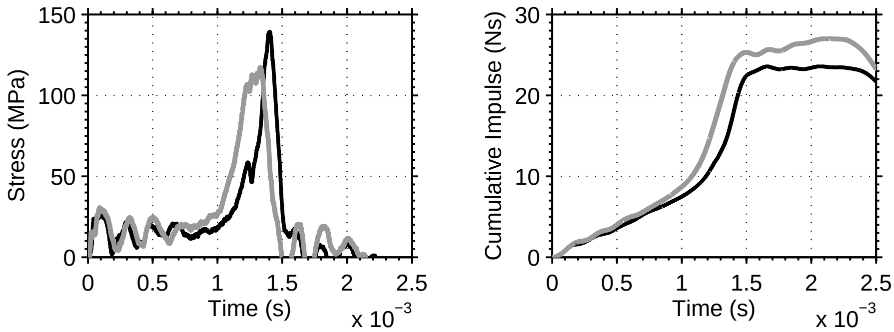

(a) (b)

Figure 16: Experimental distal face (black line) and impact face (grey line) (a) stress and (b) cumulative impulse time histories of the five-layer diamond lattice structure specimen induced by the steel impactor fired at velocities of 19.4 m/s and 16.6 m/s, respectively.

5. Discussion

Lattice structures have very regular periodic morphologies in contrast to the metallic foams which are stochastic, highly heterogeneous and contain many significant imperfections. Lattice structures with such a well-defined micro-structure allow us to easily pick out features on the load-deformation time histories and relate them to collapse of specific layers.

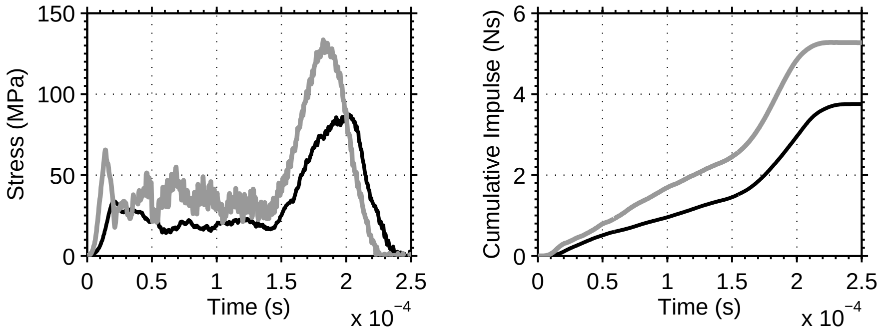

(a) (b)

Figure 17: Experimental distal face (black line) and impact face (grey line) (a) stress and (b) cumulative impulse time histories of the five-layer diamond lattice structure specimen induced by the Nylon 66 impactor fired at velocities of 178 m/s and 165 m/s, respectively.

High rate impact experiments conducted in this work provide critical data for interpretation the dynamic response of lattice structures. The low velocity HPB tests with the steel impactor on re-entrant cube samples showed that the failure of the cell layers occurred randomly without following any sequence from one end to the other. This indicates that slow application of loading causes equal distribution of load over the sample and the order of the collapse of the cell layer is controlled by the distribution of imperfections in the sample. On the other hand, the high speed HPB tests with the Nylon 66 impactor on re-entrant cube samples show that the cell layer collapse invariably runs from impact face to distal face. This indicates that load equilibrium in the specimen is not established at these higher velocities. Similar observations were reported for closed-cell Cymat/Hydro foams under dynamic loading conditions by Tan et al. (2005). Examination of crushed

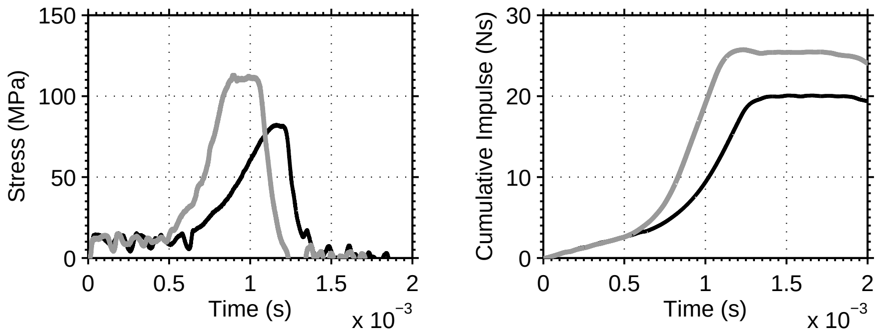

(a) (b)

Figure 18: Experimental distal face (black line) and impact face (grey line) (a) stress and (b) cumulative impulse time histories of the five-layer re-entrant cube lattice structure specimen induced by the steel impactor fired at velocities of 16.8 m/s and 19.5 m/s, respectively.

specimens following the impact tests on Cymat/Hydro foams showed that deformation is through the cumulative multiplication of discrete crush bands for static loading and for dynamic loading at sub-critical impact velocities. At super-critical impact velocities, specimens show a shock-type deformation response, where the deformation is localised behind a travelling crushing interface. Samples deform by progressive cell crushing from the impact surface. This bears analogies with propagating Lüder's bands in metal plasticity under dynamic loading. Tan et al. (2005) attributed the enhancement of the dynamic plastic collapse stress at sub-critical velocities to micro-inertial effects. In this velocity regime, the dynamic strength properties are affected by the the specimen cell-size and cell morphological defects. At super-critical impact velocities, inertia effects associated with the dynamic localisation of

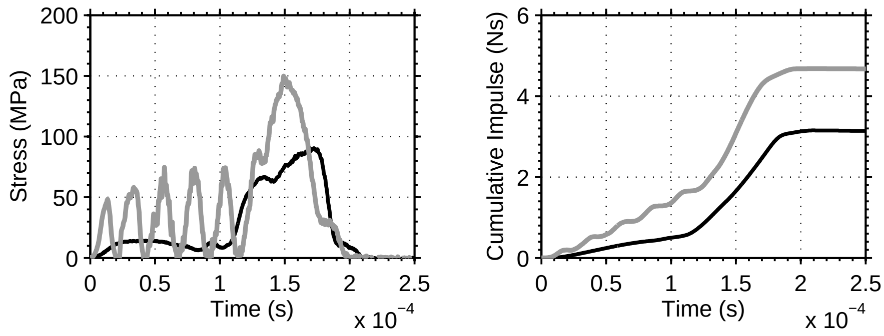

(a) (b)

Figure 19: Experimental distal face (black line) and impact face (grey line) (a) stress and (b) cumulative impulse time histories of the five-layer re-entrant cube lattice structure specimen induced by the Nylon 66 impactor fired at velocities of 134 m/s and 136 m/s, respectively.

crushing are responsible for the enhancement of the dynamic strength properties. The effects of specimen size and cell morphological defects on the measured dynamic properties are insignificant. Similarities in the dynamic response of the Cymat/Hydro foams and re-entrant cube lattice structures may be explained by the similar quasi-static response of such structures which shows sharp softening behaviour following to the peak load as observed in stretch dominated (Type II) structures.

Shock-like deformation response has also been observed in cellular structures with regular periodic geometries. Reid et al. (1983) describe the localisation behaviour of a 1-D arrangement of collapsing steel rings. The mechanism described in Figure 4 of that paper, one of collapse of the unit cells propagating from the impact face to the distal end of the specimen un-

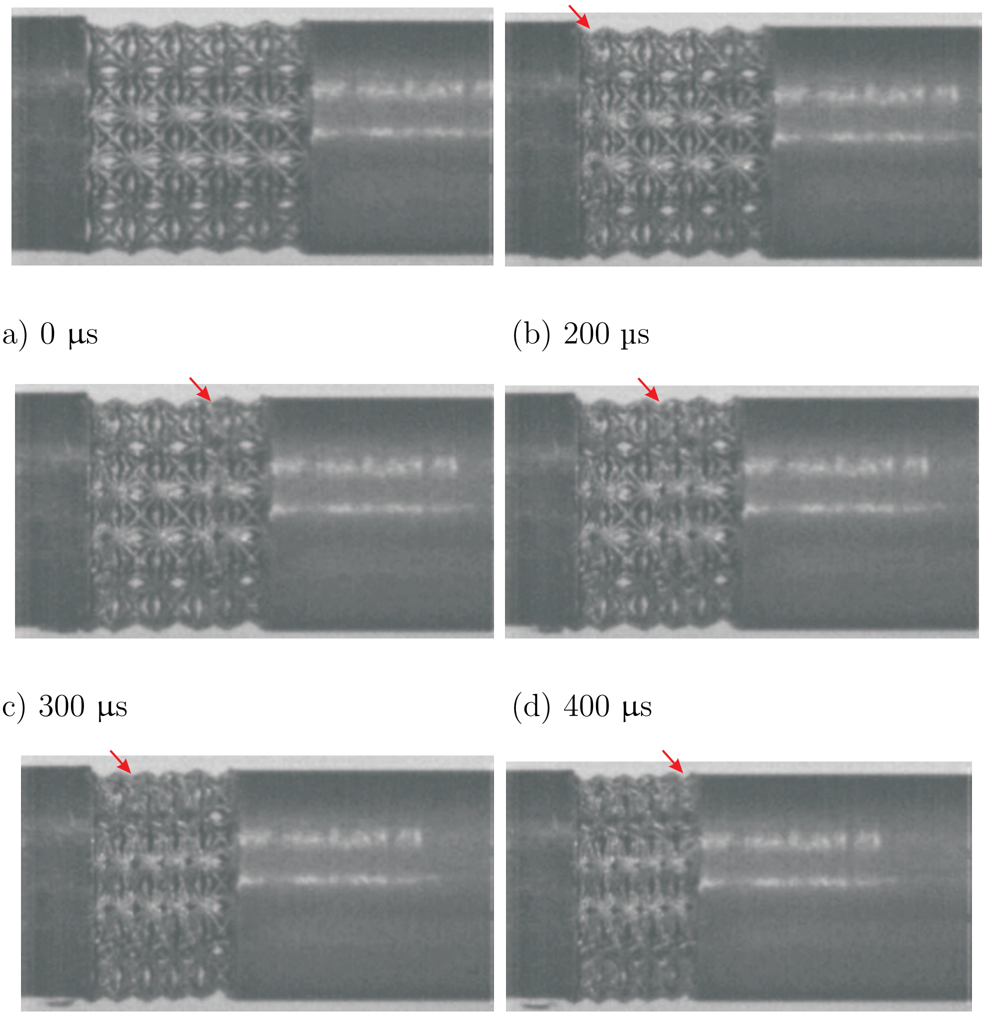

(a) 0 μs (b) 200 μs

(c) 300 μs (d) 400 μs

(e) 550 μs (f) 700 μs

Figure 20: High speed video footage of re-entrant cube specimen showing random collapse of the cell layers. The steel impactor was fired at velocity of 16.8 m/s.

der high-speed impact loading is similar to that seen in this study for Type II unit cells (Figure 21). When the impact velocity is sufficiently high to

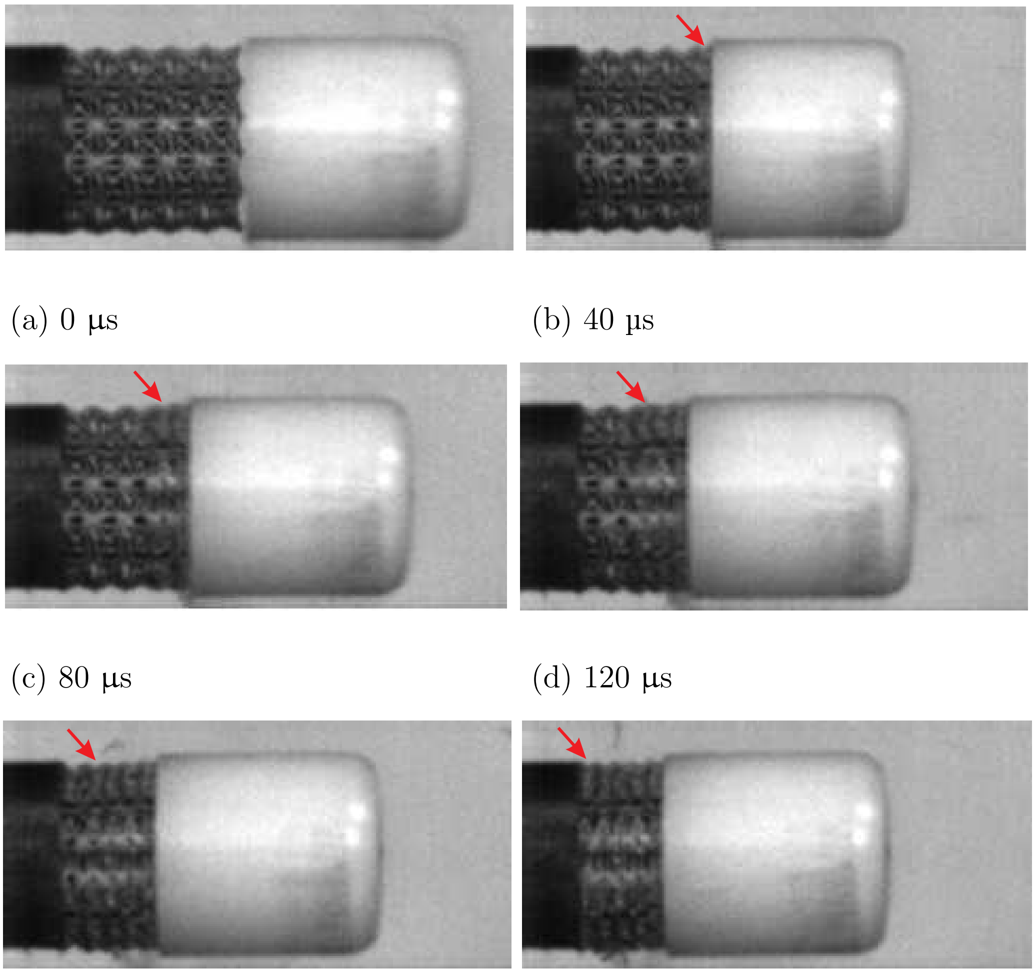

(a) 0 μs (b) 40 μs

(c) 80 μs (d) 120 μs

(e) 160 μs (f) 200 μs

Figure 21: High speed video footage of re-entrant cube specimen showing layer-by-layer collapse of the cell layers. The Nylon 66 impactor was fired at velocity of 104.0 m/s.

produce this shock-like behaviour, the successive collapse of the unit cells results in a train of loading pulses on the impact face of the specimen (Figures 17-(a) and 19-(a)). These features would presumably occur in any cellular structure collapsing under shock conditions, but are visible here due to the relatively large size of the unit cells [1]. It appears that a simple RPPL-type model will be unable to capture this shock behaviour.

6. Conclusions

An experimental study has been presented, detailing quasi-static and dynamic stress-strain behaviour of lattice specimens. The dynamic behaviour shows clear evidence of an emergent rate-dependence, with significant differences in behaviour at low and high velocities. Specifically, effectively identical impact and distal face load-time histories are seen for low velocity impacts, and significantly different response at the two faces for higher velocities. This is due to the "shock-like" response of the specimen at high velocity impacts. Whilst this in itself is not a new phenomenon, having been previously seen in experimental work on cellular polymeric and metallic foams, the relatively large and geometrically consistent form of the unit cells in this study allows direct measurement to be made of the loading features associated with the deformation and collapse of each cell layer.

Whilst previous studies have assessed the relationship between the impulse applied to a lattice specimen under dynamic loading, and the consequent structural deformation, the results presented here show how the load-time history is altered by the presence of a lattice structured cushioning layer.

[1] Presumably these features would have been apparent in the work conducted by Reid et al. Reid et al. (1983), but they didn't record the load-time history on the faces of the specimens.

In design of sacrificial protective systems, this information is necessary to allow the designer to assess the effect of the reduction in intensity of loading on a protected structure. This work also demonstrates that there is significant scope for lattice structures to serve in a number of protective applications.

7. Acknowledgements

Funding for part of this work was provided by the MOD's Armour and Protection Science and Technology Centre through project number DSTL-X1000054230. One of the authors (E. Hernandez-Nava) would like to acknowledge the support of a studentship provided by CONACyT.

References

Ashby M. The properties of foams and lattices. Philosophical Transactions of the Royal Society A 2006;364:15–30.

Reid S, Bell W, R.A. B. Structural plastic shock model for one-dimensional ring systems. International Journal of Impact Engineering 1983;1(2):175–91.

Stronge W, Shim V. Dynamic crushing of a ductile cellular array. International Journal of Mechanical Sciences 1987;29:381–400.

Reid S, Peng C. Dynamic uniaxial crushing of wood. International Journal of Impact Engineering 1997;19:531–70.

Deshpande V, Fleck N. High strain-rate compressive behaviour of aluminium alloy foams. International Journal of Impact Engineering 2000;24:277–98.

Elnasri I, Pattofatto S, Zhao H, Tsitsiris H, Hild F, Girard Y. Shock enhancement of cellular structures under impact loading: Part I experiments. Journal of the Mechanics and Physics of Solids 2007;55:2652–2671.

Harrigan J, Reid S, S. YA. The correct analysis of shocks in a cellular material. International Journal of Impact Engineering 2010;37:918–927.

Pattofatto S, Elnasri I, Zhao H, Tsitsiris H, Hild F, Girard Y. Shock enhancement of cellular structures under impact loading: Part II analysis. Journal of the Mechanics and Physics of Solids 2007;55:2672–2686.

Tan P, Reid S, Harrigan J, Zou Z, Li S. Dynamic compressive strength properties of aluminium foams. part i experimental data and observations. Journal of the Mechanics and Physics of Solids 2005;53:2174–2205.

Calladine C, English R. Strain-rate and inertia effects in the collapse of two types of energy-absorbing structure. International Journal of Mechanical Sciences 1984;26(11–12):689–701.

Zhao H, Abdennadher S. On the strength enhancement under impact loading of square tubes made from rate insensitive metals. International Journal of Solids and Structures 2004;41:6677–6697.

McKown S, Shen Y, Brookes W, Sutcliffe C, Cantwell W, Langdon G, et al. The quasi-static and blast loading response of lattice structures. Int Journal of Impact Engineering 2008;35(8):795–810.

Hasan R, Mines R, Shen E, Tsopanos S, Cantwell W, Brooks W, et al. Comparison of the drop weight impact performance of sandwich panels with aluminium honeycomb and titanium alloy micro lattice cores. Applied Mechanics and Materials 2010;24–25:413–8.

Smith M, Cantwell1 W, Guan Z, Tsopanos S, Theobald M, Nurick G, et al. The quasi-static and blast response of steel lattice structures. Journal of Sandwich Structures and Materials 2010;13(4):479–501.

U.S. Department of Transportation Federal Aviation Administration DOT/FAA/AR-00/25 . Experimental investigations material models for ti-6ai-4v titanium and 2024-t3 aluminum. 2000.

Shao F, Liu Z, Wan Y, Shi Z. Finite element simulation of machining of ti-6al-4v alloy with thermodynamical constitutive equation. The International Journal of Advanced Manufacturing Technology 2010;49(5):431–9.

Al-Bermani S, Blackmore M, Zhang W, Todd I. The origin of microstructural diversity, texture, and mechanical properties in electron beam melted ti-6al-4v. Metallurgical and Materials Transactions A 2010;41.

Hernandez-Nava E, Smith C, Derguti F, Tammas-Williams S, Leonard F, Withers P, et al. The effect of density and feature size on mechanical properties of isostructural metallic foams produced by additive manufacturing. Acta Materialia 2015;85:387–395.

Amendola A, Hernndez-Nava E, Goodall R, Todd I, Skelton R, Fraternali F. On the additive manufacturing, post-tensioning and testing of bi-material tensegrity structures. Composite Structures 2015;131:66–71.

Hyde D. Conventional Weapons Program (ConWep). U.S Army Waterways Experimental Station, Vicksburg, USA; 1991.

Tyas A, Watson A. An investigation of the frequency domain dispersion correction of pressure bar signals. International Journal of Impact Engineering 2001;25(1):87–101.